Inhibited upper ocean restratification in nonequilibrium swell conditions

T. Kukulka,[1] A. J. Plueddemann,[2] and P. P. Sullivan[3]

Received 13 June 2013; accepted 29 June 2013.

[1] Diurnal restratification of the ocean surface boundary layer (OSBL) represents a competition between mixing of the OSBL and solar heating. Langmuir turbulence (LT) is a mixing process in the OSBL, driven by wind and surface waves, that transfers momentum, heat, and mass. Observations in nonequilibrium swell conditions reveal that the OSBL does not restratify despite low winds and strong solar radiation. Motivated by observations, we use large-eddy simulations of the wave-averaged Navier-Stokes equations to show that LT is capable of inhibiting diurnal restratification of the OSBL. Incoming heat is redistributed vertically by LT, forming a warmer OSBL with a nearly uniform temperature. The inhibition of restratification is not reproduced by two common Reynolds-averaged Navier-Stokes equation models, highlighting the importance of properly representing sea-state dependent LT dynamics in OSBL models. **Citation:** Kukulka, T., A. J. Plueddemann, and P. P. Sullivan (2013), Inhibited upper ocean restratification in nonequilibrium swell conditions, *Geophys. Res. Lett.*, *40*, doi:10.1002/grl.50708.

1. Introduction

[2] The ocean surface boundary layer (OSBL) is a critical region for weather and climate systems because it couples the ocean and atmosphere through air-sea fluxes of heat, momentum, and mass [*Melville*, 1996; *Thorpe*, 2004; *Sullivan and McWilliams*, 2010]. Two key processes control the vertical structure of the OSBL: deepening due to buoyancy entrainment at the mixed layer base and shoaling during restratification associated with surface heating [*Price et al.*, 1986; *Large et al.*, 1994]. Ocean surface waves influence the OSBL structure because their Stokes drift is involved in forming wind-aligned roll vorticies, called Langmuir circulation [*Craik and Leibovich*, 1976] or Langmuir turbulence (LT) [*McWilliams et al.*, 1997]. LT is a principal component of upper ocean mixing [*Thorpe*, 2004; *Belcher et al.*, 2012]; yet, it is insufficiently understood and not represented in most upper ocean models.

[3] Significant progress has been made over the last three decades in observing [*Smith et al.*, 1992; *Farmer and Li*, 1995; *Plueddemann et al.*, 1996; *D'Asaro and Dairiki*, 1997] and modeling LT properties. State-of-the-art LT models are commonly based on turbulence resolving large-eddy simulations (LES) adopting the systematic mathematical theory by *Craik and Leibovich* [1976] [*Skyllingstad and Denbo*, 1995; *McWilliams et al.*, 1997; *Li et al.*, 2005]. LES model results have been successfully compared to observations [*Skyllingstad et al.*, 1999; *Gargett et al.*, 2004; *Li et al.*, 2009; *Kukulka et al.*, 2009, 2011; *Harcourt and D'Asaro*, 2010], but most often for cases involving mixed layer deepening associated with equilibrium wind-driven waves [*Phillips*, 1985]. Exceptions are the LES study by *Sullivan et al.* [2012], investigating transient LT under hurricanes, and the studies by *Min and Noh* [2004] and *Noh et al.* [2009], revealing the breakdown of LT under strong surface heating.

[4] Previous observations [*Weller and Price*, 1988; *Li et al.*, 1995; *Plueddemann and Weller*, 1999], two-dimensional model results [*Li and Garrett*, 1995], and LES model results [*Min and Noh*, 2004; *Noh et al.*, 2009] indicate that the enhanced vertical heat transport by LT may inhibit or delay upper ocean restratification. Specifically, it has been hypothesized that LT could be sustained under relatively low winds in the presence of gradually decaying (nonequilibrium) swell, suppressing diurnal restratification [*Plueddemann and Weller*, 1999; *Thorpe*, 2004]. Motivated by earlier observations, the goal of this study is to conduct and evaluate an idealized LES experiment that examines the role of LT in OSBL restratification under nonequilibrium swell conditions.

2. Idealized LES Experiments

[5] *Plueddemann and Weller* [1999] observed two 24 h periods of low-wind and decaying, nonequilibrium swell after relatively strong winds dropped abruptly (black lines in Figures 1a–1c). Despite significant surface heating during those periods, the OSBL did not restratify, reflected by the small temperature differences between 2.25 m and 11.25 m depth (Figure 1d). Our LES experiment is motivated by these observations; however, we do not attempt to compare the details of observations and LES, which is a much more elaborate task due to, e.g., the presence of larger-scale horizontal advection, the uncertainty in light absorption, or the effects of resonant wind forcing requiring careful choice of initial conditions.

2.1. Surface Forcing

[6] The imposed forcing consists of two phases. The initial, high-wind phase has a constant wind stress $\tau = 0.28\,\mathrm{N/m^2}$ ($U_{10} = 13\,\mathrm{m/s}$, $u_* \approx 1.7\,\mathrm{cm/s}$, where U_{10} denotes the 10 m height wind speed and u_* is the water friction velocity) and persistent cooling at about $I_0 = -200\,\mathrm{W/m^2}$, where I_0 denotes the surface heat flux. This forcing is imposed for

[1]School of Marine Science and Policy, College of Earth, Ocean, and Environment, University of Delaware, Newark, Delaware, USA.
[2]Department of Physical Oceanography, Woods Hole Oceanographic Institution, Woods Hole, Massachusetts, USA.
[3]National Center for Atmospheric Research, Boulder, Colorado, USA.

Corresponding author: T. Kukulka, School of Marine Science and Policy, College of Earth, Ocean, and Environment, University of Delaware, Newark, DE 19716, USA. (kukulka@udel.edu)

0094-8276/13/10.1002/grl.50708

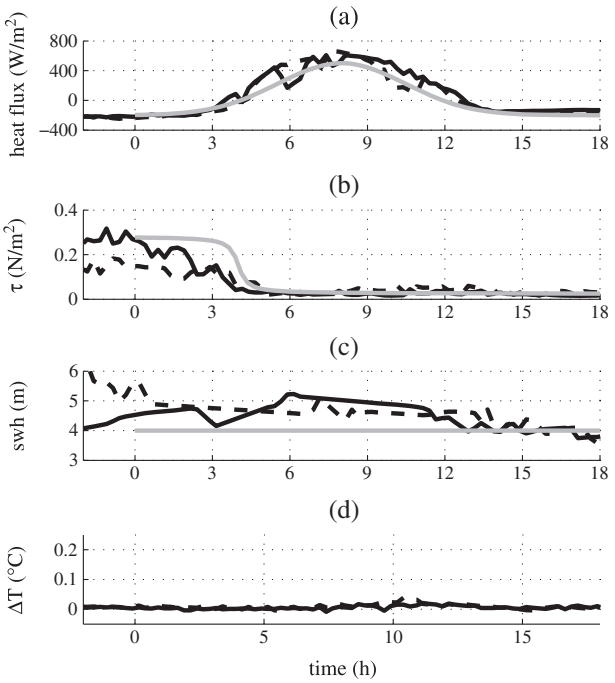

Figure 1. Observed surface forcing and upper ocean response during two heating events on 5 March (black solid) and 12 March 1990 (black dashed solid) [*Plueddemann and Weller*, 1999]. (a) Total heat flux into the ocean, (b) wind stress, and (c) significant wave height. (d) Temperature difference between 2.25 m and 11.25 m depth suggests the surface layer remains mixed in spite of significant heating. The idealized forcing imposed in the simulations (gray) starts at $t = 0$.

a duration of about 3 h, long enough so that the LES fields are fully turbulent over the OSBL at the onset of surface heating (gray lines, Figures 1a and 1b). Between hours 3 and 4, the imposed wind drops to $U_{10} = 4$ m/s ($u_* \approx 0.5$ cm/s) and remains constant thereafter. The heating phase, associated with daytime solar insolation, begins as the wind drops at $t = 4$ h and peaks at $t = 8$ h with $I_0 = 500$ W/m^2. Nighttime cooling resumes at $t = 12$ h.

[7] We modify the LES temperature equation to distribute incoming short wave radiation ($I_0 > 0$) based on a simplified model for clear ocean water following *Paulson and Simpson* [1977],

$$I(z) = I_0 R \exp(z/\zeta_1) + I_0(1-R)\exp(z/\zeta_2)), \qquad (1)$$

where z is the vertical coordinate (positive upward and $z = 0$ at surface), $R = 0.62$, $\zeta_1 = 1.5$ m, and $\zeta_2 = 20$ m.

[8] The Stokes drift is based on a constant monochromatic wave with significant wave height $H_s = 4$ m and wave length $\lambda = 70$ m, resulting in a surface Stokes drift $u_s = 16.6$ cm/s. These parameters are consistent with observations and are chosen to represent equilibrium wind-driven sea conditions for the high-wind state. Observed wind and waves were approximately unidirectional and aligned. Because of its relatively weak dissipation rate, swell does not decay significantly for several hours after an abrupt drop in wind speed [*Ardhuin et al.*, 2009] (Figure 1c), so that the initially imposed wave forcing is maintained throughout the heating phase. The turbulent Langmuir number $La_t = \sqrt{u_*/u_s}$ decreases from $La_t = 0.32$ during the high-wind phase to $La_t = 0.17$ during the heating phase, so that we expect LT to dominate shear-driven turbulence during heating [*McWilliams et al.*, 1997]. Furthermore, the wave age increases to $c_p/u_{*a} = 75$ during the heating phase, where c_p is the peak phase speed and u_{*a} the air friction velocity. This wave age reflects nonequilibrium swell conditions [*Komen et al.*, 1996] with minimal turbulence injection by breaking waves whose effect is confined to about one significant wave height for pure wind-driven seas [*Terray et al.*, 1996].

[9] For the swell conditions under consideration, breaking waves likely do not influence the OSBL dynamics at depths below 0.5 m. First, observations support a white-capping threshold for wind speeds below about 4 m/s [*Callaghan et al.*, 2008], indicating that the energy injection by bubble entraining breakers is small. Second, we estimate that the significant wind-wave height, computed from the wind-forced part of the wave spectrum [*Komen et al.*, 1996], is only about 0.5 m, i.e., much smaller than the OSBL depth. Third, LES results with a stochastic representation of breaking waves indicates that for older seas the breaking effect is mostly at the small scales and decreases rapidly with depth [*Sullivan et al.*, 2007].

2.2. Model Setup

[10] We employ the laterally periodic LES model from *McWilliams et al.* [1997] with all model modifications and details described by *Kukulka et al.* [2009, 2010]. Wave effects are captured by a vortex force that involves the Stokes drift (i.e. LT model). If the Stokes drift is set to zero, the LES model simply solves the spatially averaged Navier-Stokes equations without wave forcing but still captures shear and buoyancy instabilities (no LT model). The Coriolis force is set to zero to reduce the parameter space and to avoid complexities associated with resonant/off-resonant wind forcing due to different phases of the inertial current. Therefore, the vertically integrated volume transport is identical for the simulations with and without waves [*Kukulka et al.*, 2010].

[11] Initially, the horizontally averaged velocity field is zero and the OSBL depth h is set to $h = 25$ m, consistent with observed conditions prior to restratification [*Weller and Plueddemann*, 1996]. Below the mixed layer a stable temperature gradient of 0.02 K/m is imposed. By trial and error we determined that a horizontal domain size of 160 m $\times$ 160 m with 320 $\times$ 320 points and a 60 m deep ocean with 200 vertical points sufficed to capture (a) large turbulent structures developing during the initial high-wind speed phase and (b) small-scale turbulent eddies near the surface in the presence of a stably stratified surface layer [*Beare et al.*, 2006]. Sensitivity tests indicate that a higher resolution or larger domain size does not change the conclusions presented here. The resolved turbulent kinetic energy (TKE) contribution is usually well above 80%, even at the time of maximum heating, and always exceeds 70%, indicating that energy and flux carrying eddies are sufficiently resolved [*Pope*, 2008].

3. Results

3.1. Upper Ocean Response and Heat Transport

[12] The evolution of horizontally averaged temperature profiles (Figure 2a) reveals that with LT the OSBL only

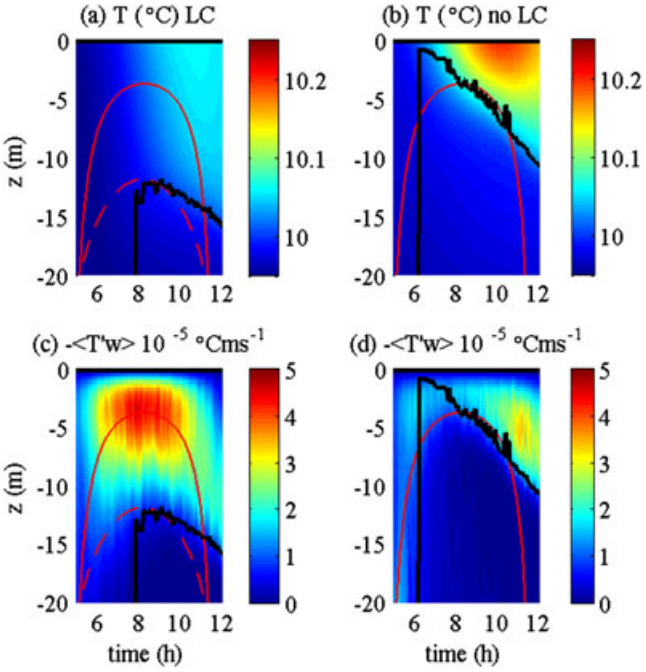

Figure 2. Evolution of (a, b) horizontally averaged temperature profiles and (c, d) simulated resolved turbulent temperature flux with LT (in Figures 2a and 2c) and without LT (Figures 2b and 2d). OSBL depth h (black line), Monin-Obukhov length L (solid red line), and L_L from (2) (dashed red line).

weakly stratifies, which is in agreement with the small observed temperature gradients (Figure 1d). This result is consistent with previous idealized model studies, which suggest that for our range of La_t and Hoenikker number $Ho = B_0\lambda/(\pi u_s u_*^2) > -0.5$, LT develops under heating and plays a key role in redistributing heat vertically and thus suppressing restratification ($B_0 = -g\alpha I_0/(\rho C_p)$ is the surface buoyancy flux, α the thermal expansion coefficient, C_p the specific heat capacity, ρ the density of water, and g the acceleration of gravity) [*Li and Garrett*, 1995; *Min and Noh*, 2004; *Noh et al.*, 2009]. Note, however, that it is not straightforward to compare the previous constant forcing model results to the transient swell conditions investigated here.

[13] Without LT, a distinct, well-stratified near-surface layer develops during the heating event (Figure 2b). Consistently, the vertical turbulent temperature flux $\langle T'w\rangle$ is significantly larger with LT than without LT (Figures 2c and 2d) (w is the vertical velocity, T is temperature, $\langle\cdot\rangle$ indicates horizontal averages, and primes denote deviations from the horizontal average).

[14] Evaluation of the instantaneous temperature flux $T'w$ in a horizontal plane of the LT model shows that coherent structures transport warmer, near-surface water downward in narrow bands that are aligned with the wind (Figure 3a). For the no LT model the heat transport is more local and intermittent, which indicates the presence of small-scale internal overturning induced by local shear instabilities (Figure 3b).

[15] To confirm that nonequilibrium swell is critical, we performed two sensitivity tests. In the first case, waves were reduced to be in equilibrium with the weaker wind after $t = 6$ h ($H_s \approx 0.4$ m and $\lambda \approx 17$ m). This resulted in much weaker LT activity and OSBL characteristics resembling closely those for the no LT model. For the second test, we eliminated the initial high-wind period, so that the wind and wave forcing was constant throughout at $U_{10} = 4$ m/s and $H_s = 4$ m. For this case results are close to the LT model.

[16] For the no LT model, the OSBL becomes very shallow shortly after the onset of heating, while with LT the OSBL does not start shallowing until the time of maximum heating (Figure 2). Without LT, the small values of h and turbulent heat flux are consistent with Monin-Obukhov similarity theory of solid wall boundary layers, where the Monin-Obukhov length $L = -u_*^3/(\kappa B_0)$ provides an estimate of the depth where TKE shear production balances buoyant destruction (conversion to potential energy). For the stably stratified boundary layer, L is related to the depth of the fully turbulent boundary layer (Figures 2b and 2d). This differs fundamentally from the LT simulation, where h and the depth of significant turbulent heat flux exceed L (Figures 2a and 2c), suggesting that LT plays a key role in the OSBL transport and TKE budgets.

3.2. Diagnosing Langmuir Turbulence

[17] Profiles of root mean square velocities (Figure 3c, dash-dotted lines) reveal the characteristic ordering of shear-driven turbulence without LT $\langle w'^2\rangle^{1/2} < \langle v'^2\rangle^{1/2} < \langle u'^2\rangle^{1/2}$, where u, v, and w are the along-wind, cross-wind, and vertical velocities, respectively [*Pope*, 2008]. With LT the ordering changes to $\langle u'^2\rangle^{1/2} < \langle v'^2\rangle^{1/2} \sim \langle w'^2\rangle^{1/2}$ typical for Langmuir turbulence [*Li et al.*, 2005]. Furthermore, the resolved turbulent Eulerian shear production without LT (dash-dotted line Figure 3d) significantly exceeds that with LT (black solid line Figure 3d). In the LT model, the dominant source of TKE is due to Stokes drift shear production, which significantly exceeds the Eulerian shear production terms with and without LT. This explains why L does not set h in the LT model.

[18] Similar to L, one may define a depth scale where the Stokes production balances the buoyant destruction. Conceptually, such a length scale is related to $L_L \sim La_t^{-2}L$, where La_t^2 approximates the ratio of Eulerian to Stokes drift TKE shear production [*McWilliams et al.*, 1997; *Belcher et al.*, 2012]. However, this estimate inaccurately scales the Stokes drift shear as $u_s/(\kappa L_L)$. A potentially more accurate estimate is obtained by retaining the exponential dependency of the Stokes drift, so that

$$L_L = \lambda(4\pi)^{-1}\ln(-4\pi[u_s u_*^2][B_0\lambda]^{-1}). \quad (2)$$

Similar to L for shear-driven turbulence, L_L determines h in the LT model (red dashed line in Figure 2). Although we do not establish the robustness of (2) as an estimator for h, (2) clearly highlights that the nondimensional parameter $(L_L B_0)/(u_s u_*^2)$ is not constant like the analogous parameter $(LB_0)/u_*^3$ without LT but depends on Ho.

4. Comparison With RANS Models

[19] The Price-Weller-Pinkel (PWP) [*Price et al.*, 1986] and K profile parameterization (KPP) [*Large et al.*, 1994] models are two common Reynolds-averaged Navier-Stokes (RANS) OSBL models, which incorporate an estimate for h based on bulk Richardson number criteria and parameterize shear instability mixing below

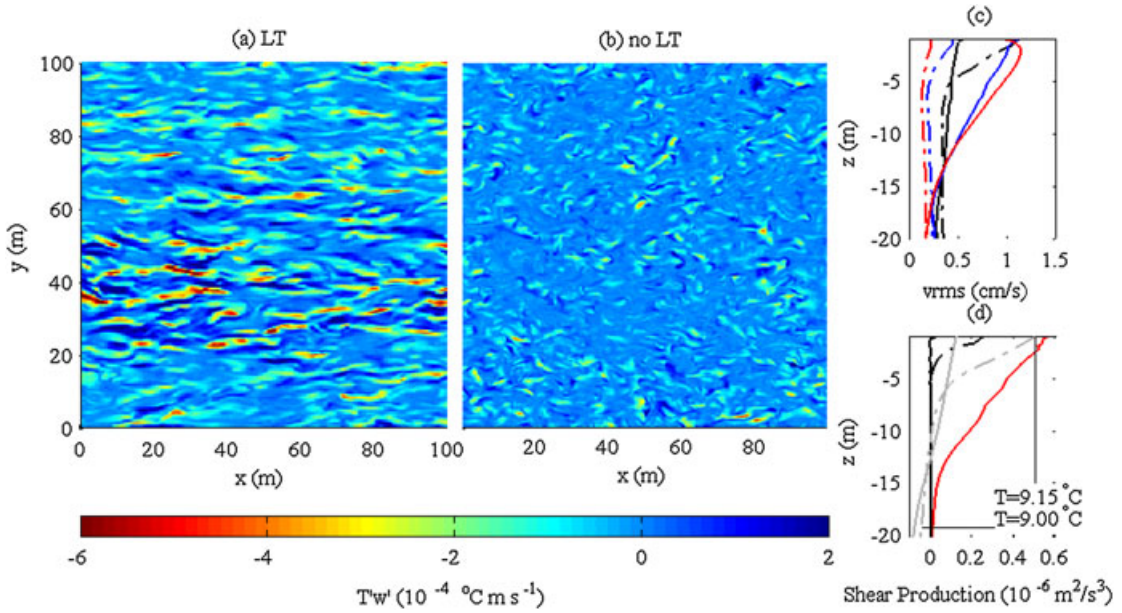

Figure 3. Instantaneous temperature flux $T'w$ at z = –2.25 m (a) with LT and (b) without LT at the time of maximum heating t = 8 h. (c) Profiles at t = 8 h of root mean square velocities ($\langle u'^2\rangle^{1/2}$ [black], $\langle v'^2\rangle^{1/2}$ [blue], $\langle w'^2\rangle^{1/2}$ [red]) with LT (solid) and without LT (dashed). (d) Profiles at t = 8 h of Eulerian shear TKE production (black) and Stokes drift shear production (red) with LT (solid) and without LT (dashed), scaled temperature profiles (gray) with LT (solid) and without LT (dashed) showing two reference values.

h based on local Richardson number criteria. In our KPP version, mixing within the OSBL is not allowed to be less than that expected from local shear instabilities, and nonlocal convective fluxes are neglected. Initial and boundary conditions and environmental parameters match the ones from the LES experiments; otherwise, the respective default RANS model parameters have been adopted. The vertical resolution equals 0.5 m.

[20] Neither RANS model captures the inhibition of restratification that is present in the observations (Figure 1d) and attributed to LT in the LES (Figure 4). This result is consistent with previous PWP modeling efforts to simulate the upper ocean response to the forcing shown in Figure 1 [*Plueddemann and Weller*, 1999]. For the default parameters, the KPP and PWP models agree reasonably well, but both show smaller stratification than found for the LES without LT. This is likely because RANS model parameters have been tuned to match ocean observations, implicitly including wave effects. For example, in the KPP model the critical Richardson number Ri_0 that parameterizes local shear instabilities is relatively large with Ri_0 = 0.7, enhancing turbulent mixing. If the theoretical value of Ri_0 = 0.25 is applied instead, the KPP model results agree more closely with the LES without LT (Figure 4).

5. Conclusions

[21] LES results based on the wave-averaged Navier-Stokes equations provide evidence for the hypothesis that the enhanced vertical heat transport by LT inhibits upper ocean restratification in low-wind, nonequilibrium swell conditions. Such conditions may be found for a diurnal heating cycle during which decaying swell persists following a rapid drop in wind speed. These conditions also effectively isolate LT dynamics in the bulk OSBL because they minimize turbulence generation due to buoyancy, Eulerian shear currents, and breaking waves (breaking wave effects are likely confined to a shallow near-surface region).

[22] Because of the enhanced TKE production due to Stokes drift shear, Monin-Obukhov similarity theory is not applicable. Analogous to the Monin-Obukhov length, we define a depth scale at which buoyancy destruction of TKE balances Stokes drift shear production and which confines the OSBL. Such a length scale provides guidance in parameterizing LT effects in RANS OSBL approaches, which commonly do not capture the observed inhibition of restratification. Our results indicate that a general LT parameterization [e.g., *Li et al.*, 1995; *Smyth et al.*, 2002; *Kantha and*

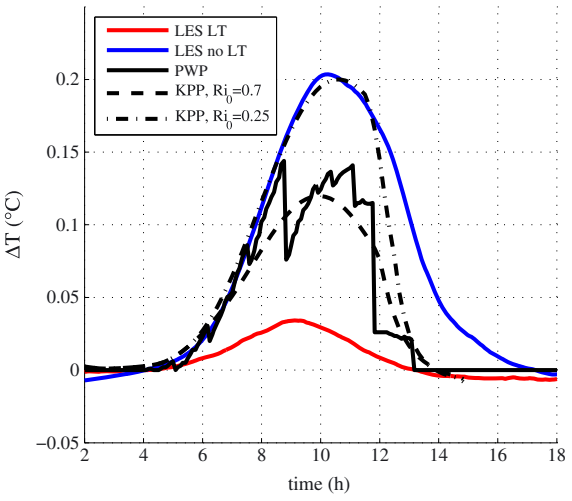

Figure 4. Comparison of LES and RANS modeled temperature differences between 2.25 m and 11.25 m depth for the idealized experiment.

Clayson, 2004; *McWilliams et al.*, 2012] should be sea-state dependent and capture nonlocal transport and Stokes drift shear production.

[23] **Acknowledgments.** We would like to thank Yign Noh for stimulating discussions and suggestions. We also appreciate valuable comments from two anonymous reviewers. This work was supported by the U.S. National Science Foundation (Grant OCE-1130678). We acknowledge computational and staff resources from IT at the University of Delaware.

[24] The Editor thanks two anonymous reviewers for their assistance in evaluating this paper.

References

Ardhuin, F., B. Chapron, and F. Collard (2009), Observation of swell dissipation across oceans, *Geophys. Res. Lett.*, *36*, L06607, doi:10.1029/2008GL037030.

Beare, R. J., et al. (2006), An intercomparison of large-eddy simulations of the stable boundary layer, *Boundary Layer Meteorol.*, *118*, 247–272, doi:10.1007/s10546-004-2820-6.

Belcher, S. E., et al. (2012), A global perspective on Langmuir turbulence in the ocean surface boundary layer, *Geophys. Res. Lett.*, *39*, L18605, doi:10.1029/2012GL052932.

Callaghan, A., G. de Leeuw, L. Cohen, and C. D. O'Dowd (2008), Relationship of oceanic whitecap coverage to wind speed and wind history, *Geophys. Res. Lett.*, *35*, L23609, doi:10.1029/2008GL036165.

Craik, A. D. D., and S. Leibovich (1976), A rational model for Langmuir circulations, *J. Fluid Mech.*, *73*, 401–426.

D'Asaro, E. A., and G. T. Dairiki (1997), Turbulence intensity measurements in a wind-driven mixed layer, *J. Phys. Oceanogr.*, *27*(9), 2009–2022, doi:10.1175/1520-0485(1997)027<2009:TIMIAW>2.0.CO;2.

Farmer, D., and M. Li (1995), Patterns of bubble clouds organized by Langmuir circulation, *J. Phys. Oceanogr.*, *25*, 1426–1440.

Gargett, A. E., J. Wells, A. E. Tejada-Martinez, and C. E. Grosch (2004), Langmuir supercells: A mechanism for sediment resuspension and transport in shallow seas, *Science*, *306*, 1925–1928.

Harcourt, R. R., and E. A. D'Asaro (2010), Measurement of vertical kinetic energy and vertical velocity skewness in oceanic boundary layers by imperfectly lagrangian floats, *J. Atmos. Oceanic Technol.*, *27*, 1918–1935.

Kantha, L. H., and C. A. Clayson (2004), On the effect of surface gravity waves on mixing in the oceanic mixed layer, *Ocean Model.*, *6*, 101–124.

Komen, G. J., et al. (eds.) (1996), *Dynamics and Modelling of Ocean Waves*, 532 pp. 1st edn, Cambridge Univ. Press, Cambridge, Great Britain.

Kukulka, T., A. J. Plueddemann, J. H. Trowbridge, and P. P. Sullivan (2009), Significance of Langmuir circulation in upper ocean mixing: Comparison of observations and simulations, *Geophys. Res. Lett.*, *36*, L10603, doi:10.1029/2009GL037620.

Kukulka, T., A. J. Plueddemann, J. H. Trowbridge, and P. P. Sullivan (2010), Rapid mixed layer deepening by the combination of Langmuir and shear instabilities: A case study, *J. Phys. Oceanogr.*, *40*(11), 2381–2400, doi:10.1175/2010JPO4403.1.

Kukulka, T., A. J. Plueddemann, J. H. Trowbridge, and P. P. Sullivan (2011), The influence of crosswind tidal currents on Langmuir circulation in a shallow ocean, *J. Geophys. Res.*, *116*, C08005, doi:10.1029/2011JC006971.

Large, W., J. McWilliams, and S. Doney (1994), Ocean vertical mixing: A review and a model with a nonlocal boundary layer parameterization, *Rev. Geophys.*, *32*(4), 363–403.

Li, M., and C. Garrett (1995), Is Langmuir circulation driven by surface waves or surface cooling? *J. Phys. Oceanogr.*, *25*, 64–76, doi:10.1175/1520-0485(1995)025<0064:ILCDBS>2.0.CO;2.

Li, M., K. Zahariev, and C. Garrett (1995), Role of Langmuir circulation in the deepening of the ocean surface mixed layer, *Science*, *270*(5244), 1955–1957.

Li, M., C. Garrett, and E. Skyllingstad (2005), A regime diagram for classifying turbulent large eddies in the upper ocean, *Deep Sea Res. I*, *52*(2), 259–278.

Li, M., S. Vagle, and D. M. Farmer (2009), Large eddy simulations of upper-ocean response to a midlatitude storm and comparison with observations, *J. Phys. Oceanogr.*, *39*, 2295–2309, doi:10.1175/2009JPO4165.1.

McWilliams, J. C., P. P. Sullivan, and C. H. Moeng (1997), Langmuir turbulence in the ocean, *J. Fluid Mech.*, *334*, 1–30.

McWilliams, J. C., E. Huckle, J.-H. Liang, and P. P. Sullivan (2012), The wavy Ekman layer: Langmuir circulations, breakers, and Reynolds stress., *J. Phys. Oceanogr.*, *42*, 1793–1816.

Melville, W. K. (1996), The role of surface-wave breaking in air–sea interaction, *Annu. Rev. Fluid Mech.*, *28*, 279–321.

Min, H. S., and Y. Noh (2004), Influence of the surface heating on Langmuir circulation, *J. Phys. Oceanogr.*, *34*, 2630–2641, doi:10.1175/JPOJPO-2654.1.

Noh, Y., G. Goh, S. Raasch, and M. Gryschka (2009), Formation of a diurnal thermocline in the ocean mixed layer simulated by les, *J. Phys. Oceanogr.*, *39*(4), 1244–1257, doi:10.1175/2008JPO4032.1.

Paulson, C. A., and J. J. Simpson (1977), Irradiance measurements in the upper ocean, *J. Phys. Oceanogr.*, *7*, 952–956.

Phillips, O. (1985), Spectral and statistical properties of the equilibrium range in wind-generated gravity waves, *J. Fluid Mech.*, *156*, 505–531.

Plueddemann, A., J. Smith, D. Farmer, R. Weller, W. Crawford, R. Pinkel, S. Vagle, and A. Gnanadesikan (1996), Structure and variability of Langmuir circulation during the surface waves processes program, *J. Geophys. Res.*, *101*(C2), 3525–3543.

Plueddemann, A. J., and R. A. Weller (1999), Structure and evolution of the oceanic surface boundary layer during the surface waves processes program, *J. Mar. Syst.*, *21* (1-4), 85–102, doi:10.1016/S0924-7963(99)00007-X.

Pope, S. B. (2008), *Turbulent Flows*, 771 pp. 5th edn, Cambridge University Press, Cambridge, UK.

Price, J., R. Weller, and R. Pinkel (1986), Diurnal cycling: Observations and models of the upper ocean response to diurnal heating, cooling, and wind mixing, *J. Geophys. Res.*, *91*(C7), 8411–8427.

Skyllingstad, E., and D. Denbo (1995), An ocean large-eddy simulation of Langmuir circulations and convection in the surface mixed layer, *J. Geophys. Res.*, *100*(C5), 8501–8522.

Skyllingstad, E. D., W. D. Smyth, J. Moun, and H. Wijesekera (1999), Upper-ocean turbulence during a westerly wind burst: A comparison of large-eddy simulation results and microstructure measurements, *J. Phys. Oceanogr.*, *29*(1), 5–28.

Smith, S. D., et al. (1992), Sea surface wind stress and drag coefficients: The HEXOS results, *Boundary Layer Meteorol.*, *60*, 109–142.

Smyth, W. D., E. D. Skyllingstad, G. B. Crawford, and H. Wijesekera (2002), Nonlocal fluxes and stokes drift effects in the K-profile parameterization, *Ocean Dyn.*, *52*, 104–115, doi:10.1007/s10236-002-0012-9.

Sullivan, P. P., and J. C. McWilliams (2010), Dynamics of winds and currents coupled to surface waves, *Annu. Rev. Fluid Mech.*, *42*, 19–42, doi:10.1146/annurev-fluid-121108-145541.

Sullivan, P. P., J. C. McWilliams, and W. K. Melville (2007), Surface gravity wave effects in the oceanic boundary layer: Large-eddy simulation with vortex force and stochastic breakers, *J. Fluid Mech.*, *593*, 405–452.

Sullivan, P. P., L. Romero, J. C. McWilliams, and W. K. Melville (2012), Transient evolution of Langmuir turbulence in ocean boundary layers driven by hurricane winds and waves, *J. Phys. Oceanogr.*, *42*, 1959–1980, doi:10.1175/JPO-D-12-025.1.

Terray, E., M. Donelan, Y. Agrawal, W. Drennan, K. Kahma, A. Williams, P. Hwang, and S. Kitaigorodskii (1996), Estimates of kinetic energy dissipation under breaking waves, *J. Phys. Oceanogr.*, *26*, 792–807.

Thorpe, S. A. (2004), Langmuir circulation, *Annu. Rev. Fluid Mech.*, *36*, 55–79, doi:10.1146/annurev.fluid.36.052203.071431.

Weller, R. A., and A. J. Plueddemann (1996), Observations of the vertical structure of the oceanic boundary layer, *J. Geophys. Res. Oceans*, *101*(C4), 8789–8806, doi:10.1029/96JC00206.

Weller, R. A., and J. F. Price (1988), Langmuir circulation within the oceanic mixed layer, *Deep Sea Res. Part A*, *35*(5), 711–747, doi:10.1016/0198-0149(88)90027-1.